

# Locating TeV $\gamma$ -ray Sources with Sub-Arcminute Precision: the Pointing Calibration of the HEGRA System of Imaging Atmospheric Cherenkov Telescopes

G. Pühlhofer, A. Daum, G. Hermann, M. Heß, W. Hofmann,  
C. Köhler, M. Panter

*Max-Planck-Institut für Kernphysik, P.O. Box 103980, D-69029 Heidelberg,  
Germany*

---

## Abstract

Stereoscopic viewing of TeV  $\gamma$ -ray air showers with systems of Imaging Atmospheric Cherenkov Telescopes (IACTs) allows to reconstruct the origin of individual primary particles with an accuracy of  $0.1^\circ$  or better. The shower impact point can be determined within 15 meters. To actually achieve this resolution, the pointing of the telescopes of an IACT system needs to be controlled with high precision. For the HEGRA IACT system, a procedure to calibrate telescope pointing was established, using bright stars distributed over the sky as references. On the basis of these measurements, one determines parameters of a correction function which is valid for the complete hemisphere. After correction a pointing accuracy of  $0.01^\circ$  is achieved.

---

## 1 Introduction

The imaging Cherenkov technique has proven the most powerful tool for the detection of air showers induced by TeV  $\gamma$ -rays. Several sources have been detected in the last few years [1].

A Cherenkov telescope uses a (usually tessellated) mirror to project the Cherenkov light emitted by the air shower particles into a camera. The camera consists of a matrix of photomultipliers (PM) which record the Cherenkov light flash, efficiently rejecting night-sky background photons due to the short gating times. The image represents a 2-dimensional projection of the shower. The image shape is used to discriminate between  $\gamma$ -ray showers and hadron induced showers which cause a background signal of 99.9% of the total rate.

The position of the image in the camera determines an area on the sky where the primary came from.

The most common analysis technique for single-telescope data (see, e.g., [2,3,4]) is mainly applicable to the search for point sources. The  $\alpha$  parameter - the angle between the vector from the image center of gravity to the image of a candidate point source, and the image axis - is used to select events pointing to the source image. In such analyses, telescope mispointing can be tolerated up to  $\approx 0.1^\circ$ , without drastic loss in performance [4].

Stereoscopic viewing of showers with two or more telescopes yields far more detailed and unambiguous information about each TeV event. It allows the determination of the origin of the primary  $\gamma$  particle with an accuracy of better than  $0.1^\circ$ . The shower core which is defined as the virtual impact point of the primary onto the ground can be reconstructed within 15 meters. Besides that one gains very precise information about the energy of the primary and about its nature. By averaging over many events, source locations can be determined with subarcminute accuracy [5,6,7].

The HEGRA<sup>1</sup> collaboration has built a system of six Imaging Atmospheric Cherenkov Telescopes [8], of which up to now four telescopes run in coincident stereoscopic mode; the other two are operated independently. The following paper deals with the pointing calibration procedure which had to be developed in order to reach the intrinsic resolution of the stereoscopic system.

Section 2 briefly describes the mounts of the HEGRA IACTS and the telescope tracking philosophy. In section 3 the procedure for pointing calibration is described. Section 4 presents the model which is used to parametrise the telescopes' mispointing. In Section 5 the results of the calibrations made so far are discussed, especially concerning the mechanical performance of the telescope mounts. Section 6 demonstrates the quality of the pointing calibration by its application to data of two TeV  $\gamma$ -ray sources, the Crab pulsar and the active galaxy Mkn 501.

## 2 Telescope mounts and tracking

Each telescope of the HEGRA IACT system has an azimuthal mount with 30 mirrors arranged in the so-called Davies-Cotton design [9]. The total mirror area is  $A = 8.5 \text{ m}^2$ , the mirror dish has a diameter of  $D = 3.4 \text{ m}$  and a focal

---

<sup>1</sup> HEGRA stands for High Energy Gamma Ray Astronomy, a collaboration of Max Planck Institutes for Nuclear Physics in Heidelberg and for Physics in Munich, Universities of Kiel, Hamburg and Madrid, BUGH Wuppertal, and Yerevan Physics Institute

length of  $f = 4.90$  m. The camera is mounted in the primary focus, and consists of 271 PMs in a hexagonal pattern. Its field of view (FOV) is  $4.3^\circ$ ; each pixel covers  $0.25^\circ$  opening angle.

The telescope axes are driven by stepper motors; one step turns the telescope by  $1.3''$ . The axes' positions are monitored by optical shaft encoders whose resolution is  $1.3'$ . Tracking is computer controlled; the algorithm uses a combination of calculated driving velocity and position feedback of the shaft encoders to steer the motors. This keeps the telescopes smoothly on track within  $\pm 1$  shaft encoder tick.

A rough ( $\approx 0.1^\circ$ ) offline check of tracking performance can be applied if stars of sufficient brightness appear in the FOV during data taking. Star images can be reconstructed using the DC currents in the PMs. However the reconstruction accuracy depends on the relation of point spread function<sup>2</sup> to the pixel size. If the point spread function is small compared to the pixel size (as it should ideally be the case), the image cannot be localized to better than the pixel size. Only with a wider point spread function, the center of gravity of the currents of several adjacent pixels provides a better measure. Even in this case problems arise for irregular point spread functions, as observed near the edge of the FOV. For telescopes such as the HEGRA IACTs, with a relatively narrow point spread function [10], it is therefore inconvenient to use stars for online tracking control.

With the initial data from the HEGRA IACT system, the need for an improved calibration of telescope pointing became obvious:

- Since pointing deviations translate directly into deviations in the reconstructed shower directions - for certain geometries even with significant amplification factors - the pointing accuracy should be about one order of magnitude better than the air shower reconstruction accuracy which is better than  $0.1^\circ$  [6,7]. No significant systematic errors should remain, which could shift a point source, or smear out a signal.
- Pointing corrections should be understood in terms of a model of (mainly mechanical) error sources. Such a description allows to reliably interpolate the corrections in between a finite set of calibration points. One can monitor the time variation of the relevant parameters of mount and drive, and may ultimately be able to cure problems at their origin.

---

<sup>2</sup> defined as the spot size in the camera caused by a point light source at infinity, such as a star

### 3 Pointing calibration

Part of the information required for the pointing corrections could be derived from TV cameras mounted on the mirror dish monitoring stars as well as bending of the camera masts. The optical path however is additionally affected by the adjustment of the mirror segments relative to the dish as well as by deformations of the mirror dish itself.

Only with star images in the PM camera the full optical path can be tested. The drawbacks stated above of this way of pointing calibration can be overcome by dedicated calibration measurements for each star, so-called *point runs*, where

- the star is focused in the camera center where the spot is regular (it can be described by a spherically symmetric 2-dimensional gaussian);
- the star image is then scanned across the central pixel, following a two-dimensional grid with spacings which are smaller than both the pixel size and the point spread function.

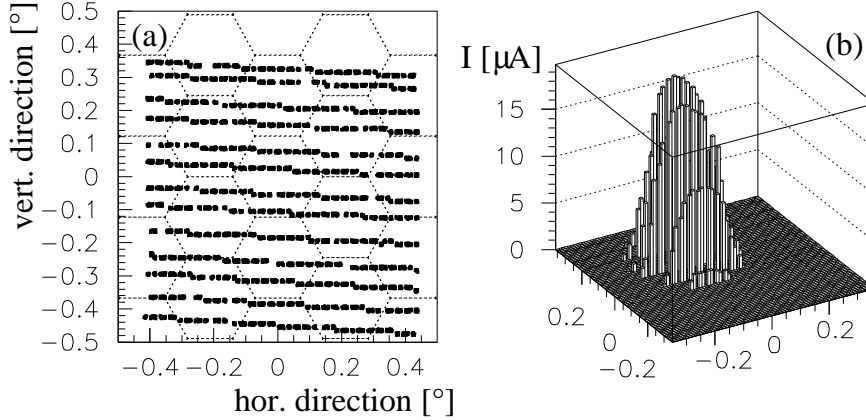


Fig. 1. Typical example of a point run, where a star is scanned across the central pixel. Each scan line is obtained by moving the azimuth motor (horizontal direction), while the altitude motor (vertical direction) is fixed<sup>3</sup>. The scanlines appear slightly rotated in the camera, because the star is moving at the same time. (a) Nominal positions of the star image in the camera, also showing the pixel outlines. (b) Current in the central pixel, as a function of the distance between the expected star image and the pixel center; one notices that the response is not centered at 0, i.e. that there is a deviation in telescope pointing.

<sup>3</sup> Horizontal and vertical coordinates refer to a coordinate system fixed to the camera. With the telescope pointing to the horizon, the horizontal direction is equivalent to azimuth, and the vertical direction equivalent to altitude.

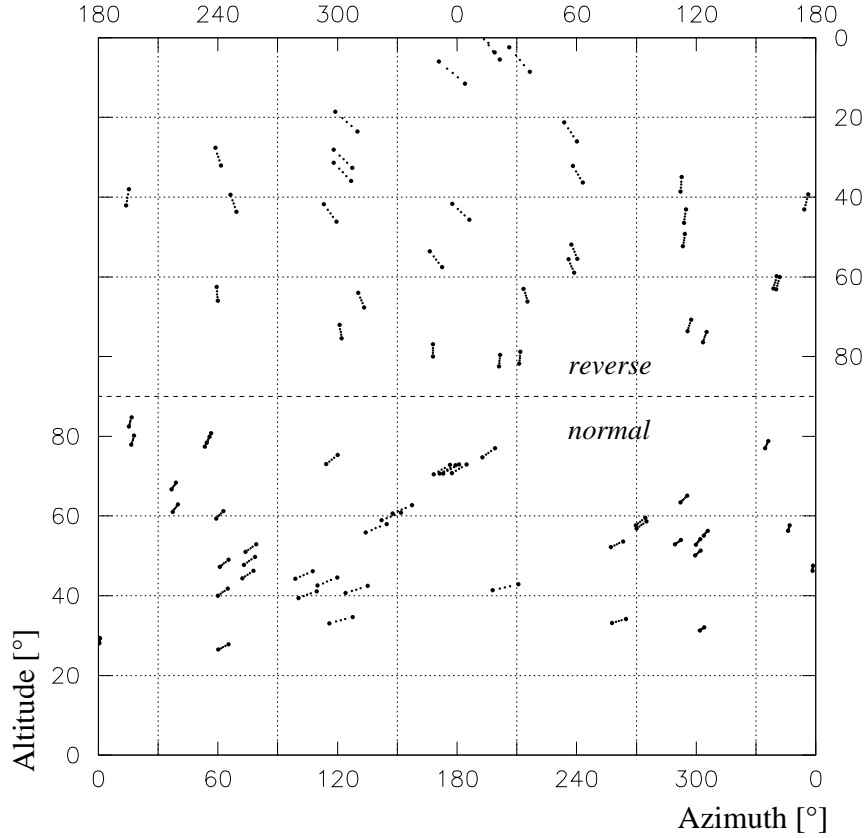


Fig. 2. Result of a pointing calibration campaign for one telescope. The measured deviations from the expected position are indicated by vectors, scaled up by a factor 50. The hemisphere is doubled due to the two operation modes (see text).

The current procedure for such point runs represents an evolution of earlier techniques such as described in [11]. To minimize the scan time, scans are taken along scan lines with fixed altitude (Fig. 1(a)). The azimuth drive is operated at constant speed, and PM currents are monitored every time the azimuth shaft encoder changes, together with the current values of the shaft encoders. A typical scan comprises 13 such scan lines, with  $0.07^\circ$  spacing in altitude, and takes about 15 min. The resulting distribution of current in the central pixel (Fig. 1(b)) is proportional to the integral of the star's image over the pixel surface. The center of the distribution determines the center of the star image and therefore the telescope pointing relative to the star. This information is then used to correct the pointing determined on the basis of shaft encoder values. The steepness of the transitions near the pixel border allows to estimate the width of the point spread function.

For stars of at least 4th (blue) magnitude, a typical point run procedure provides an accuracy of the order of better than  $0.01^\circ$  per measurement. To derive

a calibration which is valid for the complete hemisphere a set of pointruns has to be made which covers the whole sky. The result of such a calibration campaign for one telescope is shown in Fig. 2. For each pointrun the deviation from the expected position is indicated as a vector (scaled up by a factor of about 50). Due to the azimuthal mount the telescope can be driven in two modes called *normal* and *reverse* (telescope turned across the zenith), therefore the hemisphere must be examined twice.

The minimum number of pointruns is determined by the number of required parameters to describe the deviations (see section 4). Experience shows that at least 30 pointruns are needed for a new calibration which results in a total calibration time of 8 to 10 hours. For further checks of pointing performance the dataset may be reduced to a smaller number.

## 4 Modeling of pointing deviations

Various types of misalignments were considered as causes for the measured deviations; the following effects turned out to be most prominent:

- shaft encoder non-linearities;
- zero-point offsets of the shaft encoders;
- shift of the camera center with respect to the optical axis of the telescope;
- bending of telescope mount components;
- non-vertical alignment of the azimuth axis;
- non-perpendicular alignment of the altitude axis relative to the azimuth axis.

The influence of some of these parameters can be demonstrated by plotting horizontal respectively vertical deviation versus either azimuth or altitude while fixing the other coordinate. In the following two of these four plots are shown.

In Fig. 3 the horizontal deviation is plotted versus azimuth. Besides a small mean offset the main effect here is a harmonic modulation with a period of  $360^\circ$ . This can be interpreted as an error of the azimuth shaft encoder which leads to a modulation of the azimuth value; therefore the horizontal deviation decreases with increasing altitude - at the zenith an error in the azimuth value is obviously without consequences.

In Fig. 4 the vertical deviation is plotted versus altitude. For all azimuth slices a common trend is visible which is interpreted as bending of parts of the telescope mount. This leads to a deviation in the vertical direction which depends on the altitude position. The small differences at different azimuth

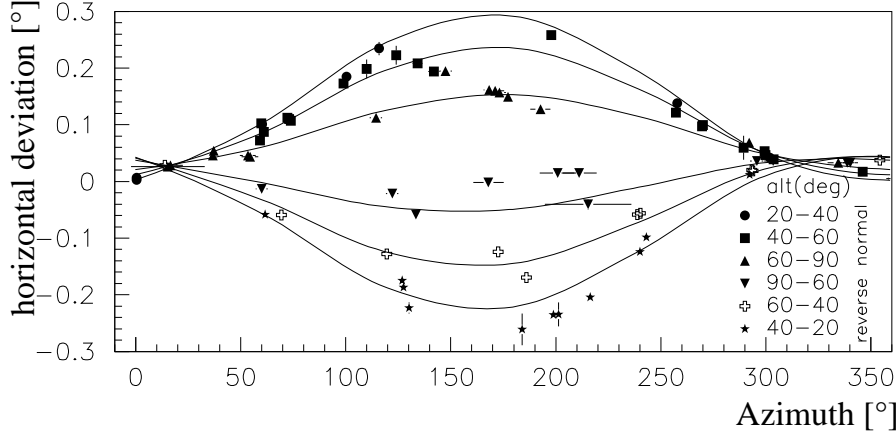


Fig. 3. Horizontal deviation vs. azimuth while applying six altitude slices. The main deviation is caused by the azimuth shaft encoder (see text).

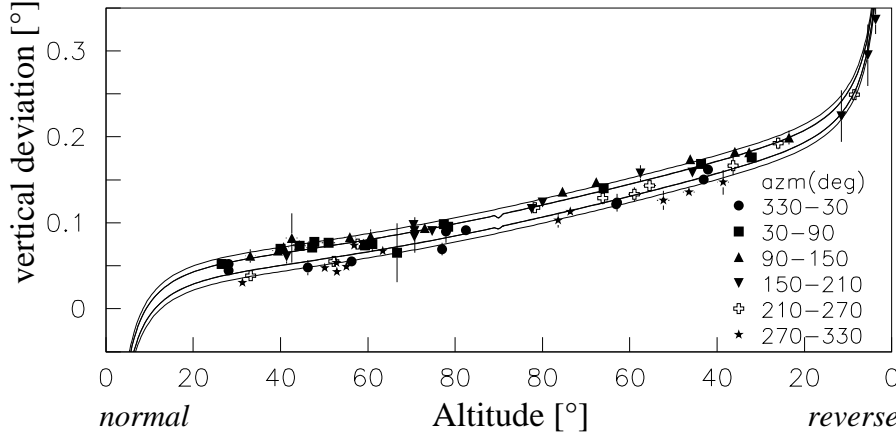


Fig. 4. Vertical deviation vs. altitude while applying six azimuthal slices. The common behaviour at all azimuth positions is caused by bending of telescope mount parts (see text).

positions are caused by the non-vertical alignment of the azimuth axis.

At small altitudes atmospheric refraction becomes visible, causing a steep variation of pointing deviations with altitude.

All the sources of pointing deviations, including atmospheric refraction, are summarized in a model where their amplitudes and, where applicable, their phases are treated as free parameters. The parameters are determined from a fit to the set of measured pointing deviations. The model can then be used to interpolate corrections between calibration points. As a measure of the quality and consistency of the model, Fig. 5 summarizes the pointing deviations before (a) and after (b) the correction function is applied. After corrections, the rms pointing error in both the horizontal (c) and vertical (d) directions is about

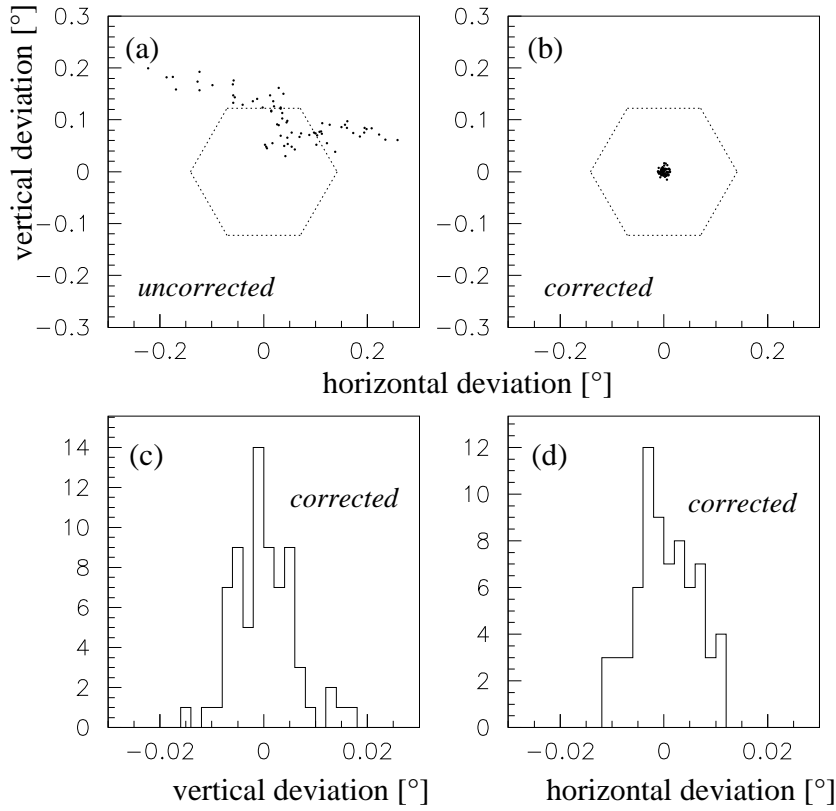


Fig. 5. The measured deviations are shown in the camera system (a) without correction, (b) after correction using the model described in the text. For reference the outline of the central pixel is superimposed. (c) and (d) show the remaining deviations in both coordinates, after correction.

$0.005^\circ$ , with a mean consistent with zero. We note that the number of fit parameters (11) is significantly smaller than the number of measured points, each of which provides two coordinates, ( $2 \times 71$  in the dataset used here for demonstration, about  $2 \times 30$  in standard new calibrations), hence this result is by no means trivial, and provides a genuine check of the model.

## 5 Results

The correction functions were determined for all four HEGRA telescopes (CT3, CT4, CT5, CT6) participating in stereoscopic mode. Table 1 shows the correction parameters which were valid in February '97. Typical errors supplied by the fit are  $0.005^\circ$  or less for the amplitudes and  $5^\circ$  for the phases, respectively. Provided that the calibration points are reasonably spread across



Telescope	CT3	CT4	CT5	CT6
maximum bending	0.039°	0.068°	0.086°	0.077°
vertical camera offset	0.049°	0.067°	−0.055°	0.059°
horizontal camera offset	0.034°	0.004°	0.053°	−0.018°
azimuth offset	−0.037°	0.002°	−0.109°	0.095°
non-vertical alignment azimuth axis				
amount	0.014°	0.039°	0.041°	0.016°
phase (sky direction)	224.8°	329.3°	199.1°	161.4°
non-linearity azimuth shaft encoder				
amplitude	0.172°	0.024°	0.030°	0.028°
phase	287.4°	308.0°	33.8°	277.2°
non-linearity altitude shaft encoder				
amplitude	0.024°	0.002°	0.154°	0.018°
phase	179.2°	180.0°	1.1°	180.1°
non-perpendicularity altitude axis	0.022°	0.045°	0.029°	0.036°

Table 1

Values of all correction parameters for CT3 - CT6 as they were valid in February 1997

Telescope	CT3	CT4	CT5	CT6
before correction				
rms horizontal	0.079°	0.023°	0.085°	0.057°
rms vertical	0.043°	0.068°	0.082°	0.065°
after correction				
rms horizontal	0.005°	0.006°	0.011°	0.005°
rms vertical	0.005°	0.006°	0.013°	0.008°

Table 2

Rms pointing deviations measured with typically 30 stars, in the horizontal and vertical directions, before and after pointing corrections, for the four HEGRA telescopes operating in stereoscopic coincidence mode.

the sky, each of the correction terms has its own distinctive signature, and the correlations between fit parameters are modest. Repeated complete calibrations demonstrated that the correction parameters are reproducible, and rather stable in time, unless hardware changes intervene (see below).

For all four telescopes, the correction scheme succeeded in reducing pointing errors from initial values of order of the pixel size, to acceptable ranges of the order of  $0.01^\circ$  or less, see Table 2. The telescope CT5 is slightly worse than the others, possibly indicative of an additional source of pointing deviations, which is not modeled in the fit.

The observed pointing deviations before correction, and hence the amplitudes of the correction parameters are typically of the order of the pixel size or less. This implies that tracking is good enough to maintain a source reasonably centered within the field of view, and that it is sufficient to apply pointing

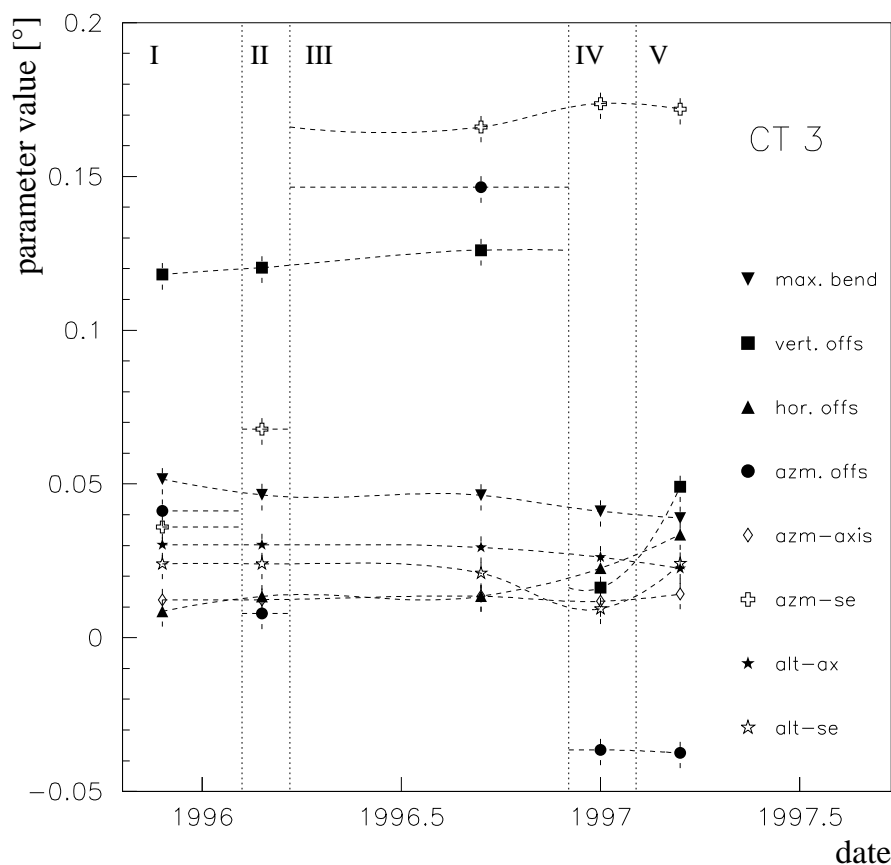


Fig. 6. Time evolution of the correction parameters of IACT 3 (only amplitudes). The dotted vertical lines separate the periods in which one correction function was valid. The dashed lines are drawn to guide the eye. Period I/II and II/III: reinstallation of azimuth shaft encoder. Period III/IV: redefinitions of shaft encoder zero positions. Period IV/V: no hardware change.

corrections offline, as first step of the analysis procedure. The great advantage of such a procedure is that after hardware changes which affect the pointing (see below) the calibration procedure can be delayed to a convenient time.

The interpretation of the parameters is straight forward. Only the modulation of the altitude shaft encoder of IACT 3, 4 and 6 (see Table 1) may also be interpreted as a common change of the bending behavior between normal and reverse mode because of similar amplitudes and phases.

Hardware changes which demand a new calibration are, for example, readjustments of mirrors or the exchange of shaft encoders. The effect of such an exchange can be seen in Fig. 6 where the time evolution of the correction parameters of telescope CT3 is shown, since the beginning of operation. Due to repair work the azimuth shaft encoder had to be reinstalled twice (between periods I,II and between II,III).

Without any preceding installation work, so far only changes in the offsets were observed. These changes are interpreted as slight changes in the mirror adjustment which lead to a broadening of the point spread function as well as to a shift of its center (p.e. Period IV/V, vertical offset).

## 6 Application to air shower observations

The pointing calibration was tested with two (within resolution) point sources of known position:

- the Crab pulsar, the TeV “standard candle”, a plerion at a distance of 8.5 kpc;
- Mkn 501, a blazar at a redshift of  $z \approx 0.03$ .

Analysis procedures and first results concerning the Crab observations were reported in [6], still using preliminary and incomplete pointing corrections. The results on  $\gamma$ -ray emission from Mkn 501, as summarized in [12], used essentially the final corrections as described in this paper.

Figs. 7(a) and (b) show the distribution of excess events in celestial coordinates. The positions of the  $\gamma$ -ray sources were determined from fits of two-dimensional Gaussian distributions to the excess. The relevant parameters of the data sets and the fit results concerning the source positions are summarized in Table 3.

The reconstructed positions differ from the radio source positions by less than 1 arcminute which is in good agreement with the expected pointing accuracy. The corresponding systematic errors are estimated from the residuals

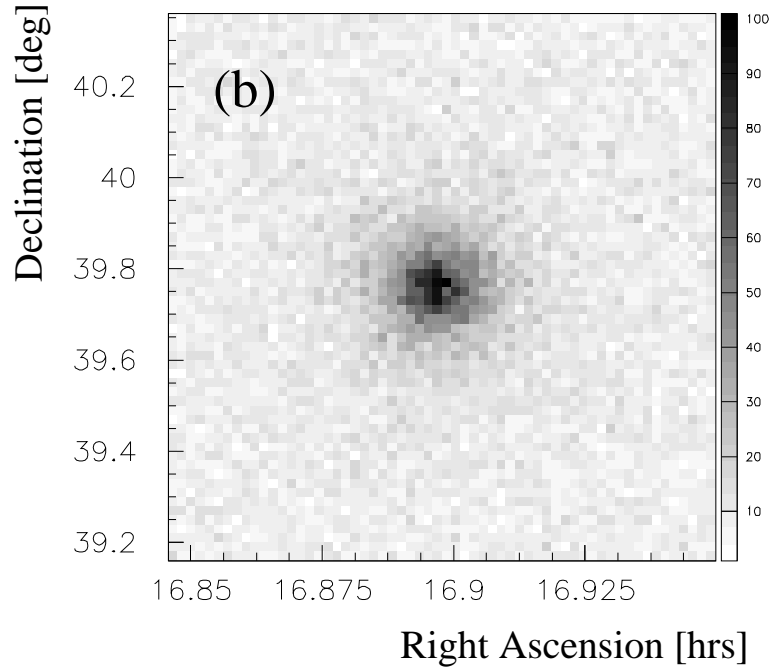
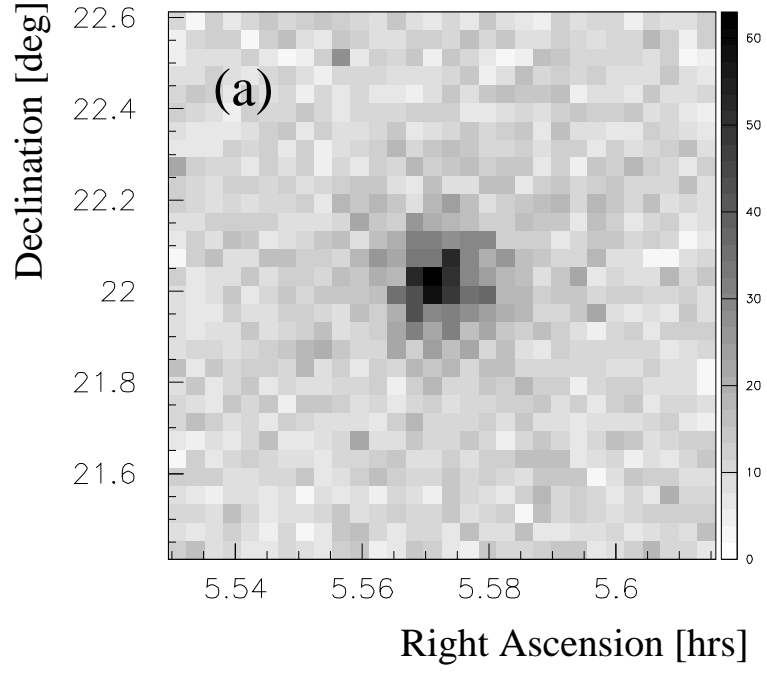


Fig. 7. Excess of  $\gamma$ -ray candidate events from the direction of the Crab nebula (a) and the blazar Mkn 501 (b). A cut on the mean width of the images, averaged over all telescopes, is used to separate  $\gamma$ -ray candidates from the uniform cosmic-ray background.

Source	Crab	Mkn 501
Observation period	12/96 - 2/97	3/97 - 5/97
On-source time	24.3 hrs	62.7 hrs
Observation mode	normal	reverse
Radio source position of current epoch		
ra	5.5725 hrs	16.8963 hrs
dec	22.013°	39.764°
$\gamma$ -ray source position		
ra	5.5720 hrs	16.8968 hrs
dec	22.020°	39.762°
Angular distance radio source - $\gamma$ -ray source		
along ra	$0.007^\circ \pm 0.007^\circ$	$0.006^\circ \pm 0.007^\circ$
along dec	$0.007^\circ \pm 0.007^\circ$	$0.002^\circ \pm 0.007^\circ$
(Gaussian) angular resolution	0.09°	0.09°

Table 3

Data sets and results of the analysis of Crab and Mkn 501 data. The errors given for the angular distances represent our estimate on systematical errors; the statistical errors are significantly smaller.

of telescope pointing after correction (see Figure 5 (c) and (d)). The angular resolution (characterized here by the Gaussian width of the distribution of excess events, projected onto one of the axes) is well below  $0.1^\circ$ <sup>4</sup>.

## 7 Summary

The HEGRA IACT system provides a spatial resolution of a new quality in TeV  $\gamma$ -ray astronomy (and even in  $\gamma$ -ray astronomy in general). The origin of an individual  $\gamma$ -ray can be reconstructed with an accuracy of better than  $0.1^\circ$ . The position of a point source of sufficient flux can be determined within  $0.01^\circ$ . To achieve this pointing quality a new calibration procedure for IACTs had to be established. It uses a set of (typically  $\geq 30$ ) pointing calibration

<sup>4</sup> In particular for the high-statistics Mkn 501 data set, the excess is not exactly Gaussian, but has a sharper peak and a more pronounced tail. Since the distribution represents a wide range of  $\gamma$ -ray energies, with the angular resolution improving at high energies, one expects such deviations from an exact Gaussian shape.

measurements distributed over the complete sky. These determine the parameters of correction functions to model the mechanical misalignments of the four telescopes which are included in the HEGRA IACTS so far. The correction functions work for the complete range in azimuth and altitude.

The precise localization of  $\gamma$ -ray sources allows better identification of counterparts in other wavebands, and may ultimately allow the precise mapping of extended sources.

## Acknowledgements

The support of the German Ministry for Research and Technology BMBF and of the Spanish Research Council CYCIT is gratefully acknowledged. We thank the Instituto de Astrofísica de Canarias for the use of the site and for providing excellent working conditions. We thank the other members of the HEGRA CT groups, who participated in the construction, installation, and operation of the telescopes. We gratefully acknowledge the technical support staff of Heidelberg, Kiel, Munich, and Yerevan.

## References

- [1] T.C. Weekes, Space Science Rev. 75 (1996) 1; M. F. Cawley and T.C. Weekes, Experimental Astronomy 6 (1996) 7.
- [2] A.M. Hillas, Proc. 19th ICRC, La Jolla, Vol. 3 (1985) 445.
- [3] M. Punch et al., Nature 358 (1992) 447.
- [4] D. Petry et al., Astron. Astrophys. 311 (1996), L13.
- [5] C.W. Akerlof et al., Astrophys. J. 377 (1991), L97.
- [6] A. Daum et al., preprint astro-ph/9704098, and Astropart. Phys., in press.
- [7] F. Aharonian et al., Astropart. Phys. 6 (1997) 343; Astropart. Phys. 6 (1997) 369.
- [8] F. Aharonian, Proceedings of the Int. Workshop “Towards a Major Atmospheric Cherenkov Detector II”, Calgary, (1993), R.C. Lamb (Ed.), p. 81.
- [9] J.M. Davies, E.S. Cotton, J. Solar Energy Sci. and Eng. 1 (1957) 16.
- [10] A. Akhperjanian et al., in preparation.
- [11] R. Mirzoyan et al., Nucl. Instr. Meth. A351 (1994) 513.
- [12] F. Aharonian et al., Astron. Astrophys. 327 (1997), L5.